RSC Advances

PAPER

View Article Online
View Journal | View Issue

Cite this: *RSC Adv.*, 2018, **8**, 25829

Significant improvement in TiO_2 photocatalytic activity through controllable ZrO_2 deposition†

Xiaofeng Wang, Rajankumar L. Patel ‡ and Xinhua Liang *

Received 21st April 2018
Accepted 6th July 2018

DOI: 10.1039/c8ra03423k

rsc.li/rsc-advances

ZrO_2 was deposited on anatase TiO_2 nanoparticles using 5–80 cycles of atomic layer deposition (ALD). The photocatalytic activity of all samples was evaluated based on the degradation of methylene blue (MB) solution under UV light. The TiO_2 sample with 45 cycles of ZrO_2 deposition (45c-Zr/TiO_2, 1.1 wt% ZrO_2) was proved to be the most efficient catalyst with a degradation kinetic constant 10 times larger than that of the pure TiO_2 sample. All samples were characterized using inductively coupled plasma atomic emission spectroscopy (ICP-AES), nitrogen adsorption–desorption, X-ray diffraction (XRD), transmission electron microscopy (TEM), UV-vis diffuse reflectance spectra analysis (UV-DRS), Raman and photoluminescence (PL) techniques. The high photocatalytic activity of 45c-Zr/TiO_2 can be attributed to stronger adsorption in the ultraviolet region and a reduction in the recombination rate of electron/hole pairs.

1. Introduction

Nowadays, TiO_2 has been widely studied as an effective photocatalyst for the degradation of organic pollutants due to its relatively high activity, chemical stability, nontoxicity and low cost.[1] However, the high recombination rate of photo-generated electrons (e^-) and holes (h^+) and slow reaction rate of pure TiO_2 have hindered its further application. Thus, the photocatalytic efficiency of TiO_2 needs to be further improved for practical and commercial use.[2]

It is well known that ZrO_2 is an n-type semiconductor with similar physico-chemical properties to those of TiO_2,[3] and therefore it has been used to prepare ZrO_2 doped TiO_2 photocatalysts because of these similar properties in order to improve the photocatalytic activity of TiO_2.[3,4] Through ZrO_2 doping, the band gap of the photocatalyst increases and the recombination rate subsequently decreases, which leads to an improvement of the photocatalytic activity. However, almost all previous studies adopted sol–gel and other similar methods to prepare ZrO_2/TiO_2, as shown in Table S1,† and thereby the crystal structure and phase composition of the samples were changed due to the mixture of Zr and Ti precursors. High ZrO_2 content would lead to poor anatase crystallinity of TiO_2 and decrease the photocatalytic efficiency; in contrast, ZrO_2 loading that is too low does not ensure an obvious increase in the band gap, and thereby the e^-/h^+ recombination rate cannot be reduced effectively. Thus, the enhancement of TiO_2 photocatalytic performance by ZrO_2 doping is restricted, and solving this dilemma is the key to further improving the activity of ZrO_2/TiO_2.

In this work, we deposited ZrO_2 on anatase TiO_2 nanoparticles (NPs) *via* different numbers of cycles (5–80) of atomic layer deposition (ALD) to investigate the effect of ZrO_2 in the photocatalytic degradation of methylene blue (MB). The samples were labeled *x*c-Zr/TiO_2, where *x* refers to the number of cycles of ZrO_2. ALD is a surface controlled layer-by-layer coating process based on self-limiting surface reactions, and it has been utilized to deposit uniform metal oxide films with sub-nanometer control of film thickness and well controlled film compositions.[5] Through making full use of the advantages of ALD, the ZrO_2 content was controlled at a low level to retain the anatase crystallinity of TiO_2 and the e^-/h^+ recombination rate decreased due to the high dispersion of ZrO_2 on the surface of TiO_2.

2. Experimental section

2.1. Preparation of ZrO_2/TiO_2 nanoparticles

ZrO_2 was deposited on TiO_2 NPs *via* ALD using tetrakis(dimethylamido)zirconium(IV) (TDMAZ) (electronic grade, ≥99.99%, Sigma-Aldrich) and deionized water as precursors in a fluidized bed reactor, as described in detail elsewhere.[6] Anatase TiO_2 NPs with an average particle size of 20 nm were purchased from US Research Nanomaterials Inc. For a typical run, 5 g of TiO_2 NPs was loaded into the reactor. The reaction temperature was 250 °C. Before the reaction, the particles were first degassed at 250 °C for 3 hours. The particle substrates were fully fluidized with a gas flow rate controlled with mass flow controllers. N_2

Department of Chemical and Biochemical Engineering, Missouri University of Science and Technology, Rolla, MO 65409, USA

† Electronic supplementary information (ESI) available: Data on photocatalytic activity, Raman and UV-visible diffuse reflectance data and a comparison of the photocatalytic activity of various photocatalysts. See DOI: 10.1039/c8ra03423k

‡ Current address: Energy and Environmental Directorate, Pacific Northwest National Laboratory, Richland, Washington 99354, USA.

was used as a flush gas to remove unreacted precursors and any byproducts during the reaction. A typical half deposition cycle used the following sequence: precursor dose, N_2 purge and evacuation. This sequence was repeated alternately for both precursors. 5 (5c-Zr/TiO_2), 25 (25c-Zr/TiO_2), 45 (45c-Zr/TiO_2), 60 (60c-Zr/TiO_2), and 80 (80c-Zr/TiO_2) cycles of ZrO_2 ALD were applied on anatase TiO_2 NPs.

2.2. Characterization

Inductively coupled plasma-atomic emission spectroscopy (ICP-AES) was used to measure the Zr mass fraction in the ZrO_2/TiO_2 samples. The surface area of the pure TiO_2 and ZrO_2-deposited TiO_2 NPs was calculated using the Brunauer–Emmett–Teller (BET) method in a relative pressure range (0.05–0.25) of nitrogen adsorption and desorption isotherms obtained using a Quantachrome Autosorb-1. The photoluminescence (PL) spectra were recorded with a HORIBA FL3-22 spectrometer (HORIBA, Edison, NJ) to evaluate the recombination rate of e^-/h^+ pairs in the samples. The morphology of ZrO_2 deposited on TiO_2 was directly observed using FEI Tecnai F20 transmission electron microscopy/energy-dispersive X-ray spectroscopy (TEM/EDS). The crystal structure of the TiO_2 and ZrO_2/TiO_2 samples was analyzed with X-ray diffraction (XRD), and the Raman spectra of the samples were recorded using a Horiba-Jobin Yvon LabRam spectrometer. UV-visible absorbance and diffuse reflectance spectra (DRS) of TiO_2 and ZrO_2/TiO_2 samples were obtained with a UV-visible spectrophotometer (Varian Cary 5). $BaSO_4$ was used as an absorbance standard. Details of the characterization are described in the ESI.†

2.3. Photocatalytic activity measurement

Degradation of MB was used to evaluate the photocatalytic performance of the TiO_2 and ZrO_2/TiO_2 samples, as described in detail previously.[7] Briefly, 0.1 g of sample was added to a 100 ml, 10 ppm MB solution. First, the solution was stirred in the dark for 60 min to ensure adsorption/desorption equilibrium. Then, the solution was irradiated using a UV lamp (360 nm UV light) and about 1 ml test sample was collected from the main solution at certain time intervals and filtered through a Millipore filter to make it particle-free for analysis using a UV-vis spectrometer (Varian Cary 50-Bio) at a 664 nm wavelength.[8] The change in concentration of MB in the main solution was recorded over a period of irradiation time.

3. Results and discussion

As shown in Fig. 1, the photodegradation efficiency of all ZrO_2/TiO_2 samples was higher than that of the pure TiO_2, and with an increasing number of ALD cycles, the photoactivity of the samples kept increasing below 45 ALD cycles of ZrO_2, then it decreased slightly with further increases in the number of ALD cycles. According to the Langmuir–Hinshelwood kinetic equation (pseudo-first-order reaction),[9] the apparent kinetic constant (k_{app}) of the 45c-Zr/TiO_2 sample reached a maximum value (0.127 min^{-1}), and its activity exceeded that of pure TiO_2 (0.012 min^{-1}) by a factor of more than ten. As shown in Table S1,† Pt ALD and CeO_2 ALD have been applied to the improvement of TiO_2 photoactivity, and they showed, at most, only a 3.0 and 3.3 times increase in photocatalytic activity compared to that of pure TiO_2, respectively.[7,10] More importantly, ZrO_2 is much cheaper and more economical for large-scale production

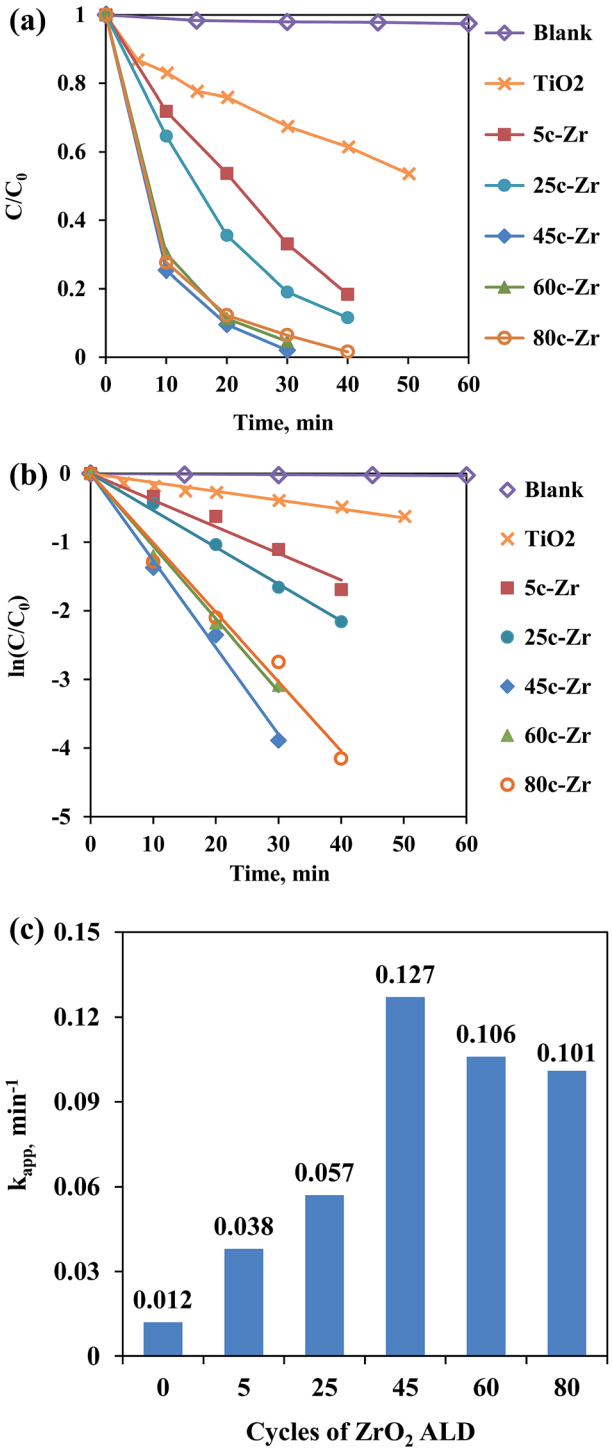

Fig. 1 (a) MB concentration and (b) relative concentration of MB as a function of UV irradiation time over different catalysts, and (c) apparent kinetic constant (k_{app}, min^{-1}) of ZrO_2/TiO_2 catalysts with different numbers of ZrO_2 ALD cycles.

compared to Pt. Compared to previously reported ZrO_2/TiO_2 photocatalysts,[4] the ALD prepared 45c-Zr/TiO_2 sample improved the photocatalytic activity of pure TiO_2 significantly, which proved that ZrO_2 ALD was one promising strategy to enhance ZrO_2/TiO_2 photocatalytic performance (Table S1†). The reasons for the much higher photoactivity of 45c-Zr/TiO_2 than that of TiO_2 in this work were investigated.

Firstly, the ZrO_2 ALD process did not affect the bulk properties of the TiO_2 NPs (*e.g.*, crystal structure and surface area). As shown in Fig. 2, the ZrO_2 content of the samples increased steadily (from 0 to 1.5 wt%) with an increasing number of ALD cycles. This is one characteristic of the ALD process. This indicates a constant growth rate of ZrO_2. The ZrO_2 loading was 0.1, 0.5, 1.1, 1.2 and 1.5 wt% in 5c-Zr/TiO_2, 25c-Zr/TiO_2, 45c-Zr/TiO_2, 60c-Zr/TiO_2, and 80c-Zr/TiO_2 samples, respectively. Since the loading of ZrO_2 deposited on the TiO_2 NPs was very low, it did not lead to an increase in particle size (decrease of surface area) or poor anatase crystallinity, which would affect the photocatalytic efficiency of the samples. In order to verify this hypothesis, the BET surface area and crystal structure of all samples were analyzed. The BET surface area remained almost constant (~70 $m^2\ g^{-1}$) even after 80 cycles of ZrO_2 ALD (Fig. 2). The large surface area can provide a lot of surface sites for the adsorption of reactant molecules.

Moreover, based on calculation, 1 g of 80c-Zr/TiO_2 contained 0.015 g ZrO_2 (5.68 g cm^{-3}) and the thickness of ZrO_2 should be around 0.038 nm (0.015/5.68/70 × 1000 nm) if ZrO_2 formed as a film on the TiO_2 NPs.[11] The thickness is much thinner than that of a real layer of ZrO_2 (>0.1 nm). Thus, ZrO_2 was highly dispersed on TiO_2 without forming a film. As shown in Fig. 3, the TEM images of 45c-Zr/TiO_2 and 80c-Zr/TiO_2 are similar to that of pure anatase TiO_2 NPs, and the lattice fringes of 0.35 nm, 0.24 nm, and 0.19 nm correspond to the (101), (004), and (200) planes of anatase, respectively.[12] No ZrO_2 film was observed, but the ICP-AES (Fig. 2) and EDS (Fig. S1†) verified the existence of Zr on the TiO_2. It seems that ZrO_2 ALD follows an island growth mechanism (Volmer–Weber mechanism) during the initial stages of the ALD process, which could be similar to that of some metal ALD processes.[13]

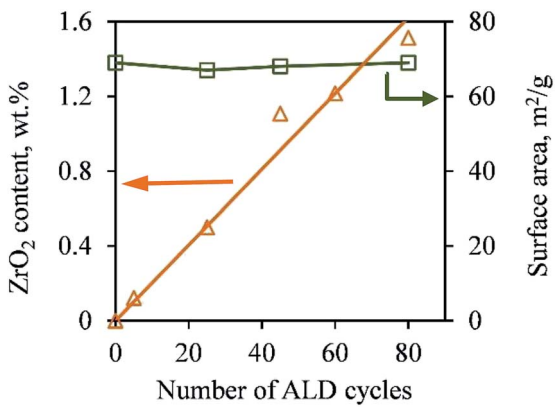

Fig. 2 ZrO_2 content and BET surface area of pure TiO_2 nanoparticles and TiO_2 nanoparticles deposited with ZrO_2 over different numbers of cycles of ALD.

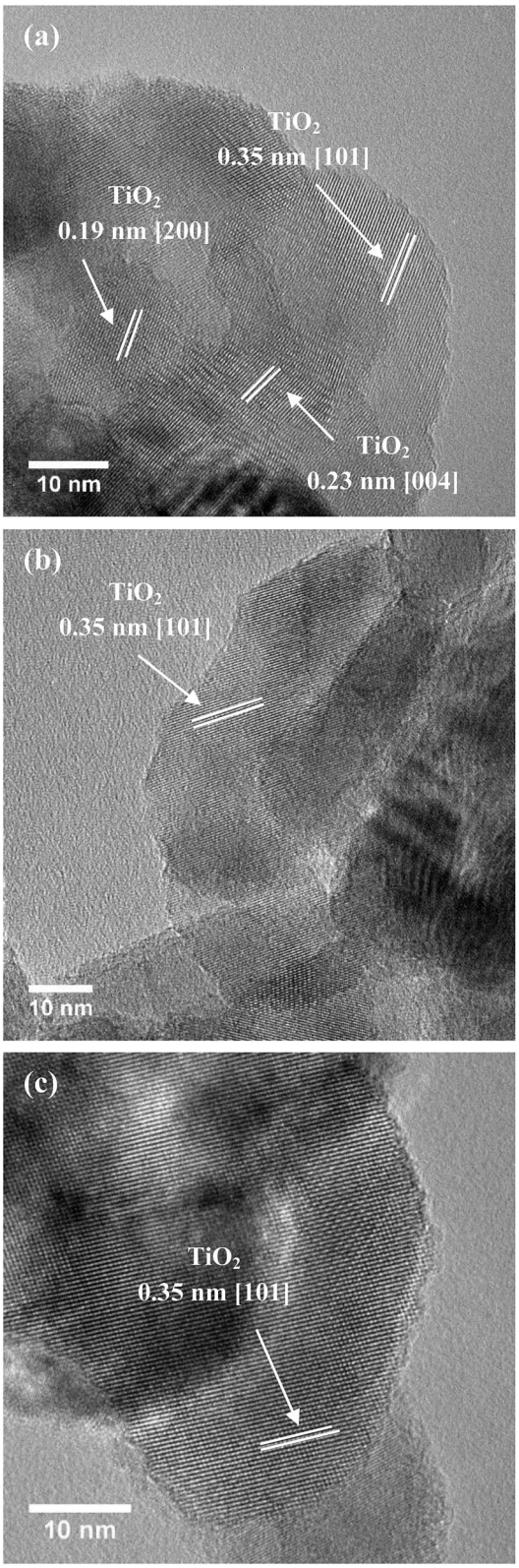

Fig. 3 TEM images of (a) TiO_2, (b) 45c-Zr/TiO_2, and (c) 80c-Zr/TiO_2 nanoparticles.

As presented in Fig. 4, the XRD patterns of all samples show peaks appearing at $2\theta = 25.3°$, 37.8°, 48.1°, 53.9°, 55.2°, 62.8° and 75.2°, corresponding to the diffraction patterns of (101),

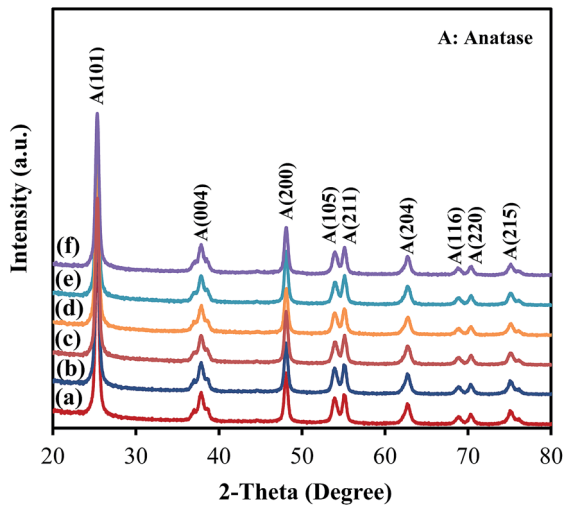

Fig. 4 XRD patterns of (a) TiO_2, (b) 5c-Zr/TiO_2, (c) 25c-Zr/TiO_2, (d) 45c-Zr/TiO_2, (e) 60c-Zr/TiO_2 and (f) 80c-Zr/TiO_2.

(004), (200), (105), (211), (204) and (215), respectively, of the pure tetragonal phase of anatase TiO_2.[14] There was no significant difference in any sample. The TiO_2 in all samples retained the anatase structure after ZrO_2 ALD and no peak corresponded to reflections from ZrO_2, which could be due to the low loading and amorphous structure of ZrO_2 on TiO_2. According to the XRD analysis, the TiO_2 crystal size was around 19 nm for all samples, which is close to the actual particle size of TiO_2 (~20 nm). Raman analysis was also performed, and all samples showed three major Raman bands at 397, 517, and 640 cm^{-1} (Fig. 5), which are attributed to the Raman-active modes of the TiO_2 anatase phase with symmetries of B1g, A1g, and Eg, respectively.[15] Thus, our hypothesis that the surface area and anatase crystallinity of TiO_2 did not change after the ALD process was proved.

Secondly, a larger band gap corresponds to stronger redox ability, which leads to a reduction in the e^-/h^+ recombination rate and an improvement in photocatalytic activity. Since the band gap of ZrO_2 is around 4.6 eV and is larger than that of anatase TiO_2 (3.2 eV),[16] the band gap of ZrO_2/TiO_2 samples was enlarged after ZrO_2 ALD.[17] As shown in Fig. 6, S2 and S3,† the band gap of the samples kept increasing along with increasing numbers of ALD cycles, which is consistent with previous reports.[4d,18] Because the photocatalytic degradation process can

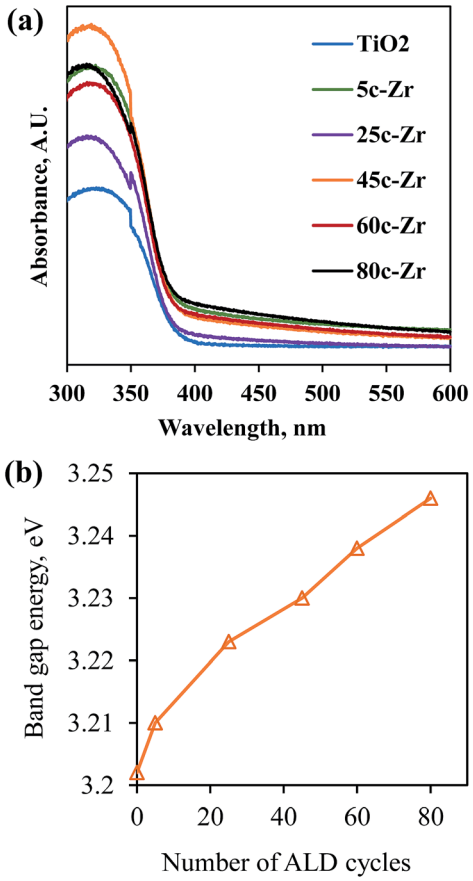

Fig. 6 (a) UV-visible absorption spectra, and (b) the band gap energy of the TiO_2 and ZrO_2/TiO_2 samples.

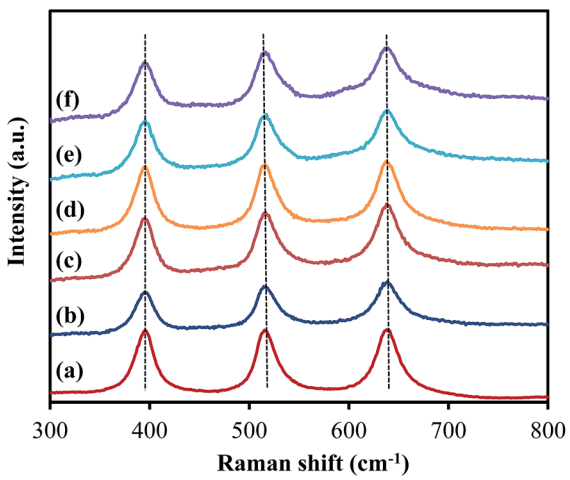

Fig. 5 Raman spectra of (a) TiO_2, (b) 5c-Zr/TiO_2, (c) 25c-Zr/TiO_2, (d) 45c-Zr/TiO_2, (e) 60c-Zr/TiO_2 and (f) 80c-Zr/TiO_2.

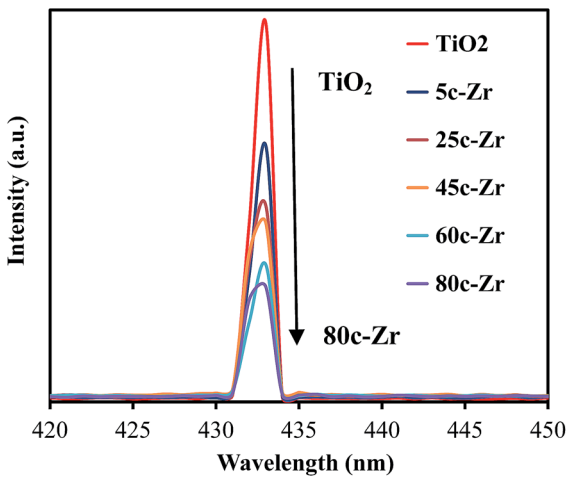

Fig. 7 Photoluminescence spectra of TiO_2 and ZrO_2/TiO_2 samples excited at 280 nm.

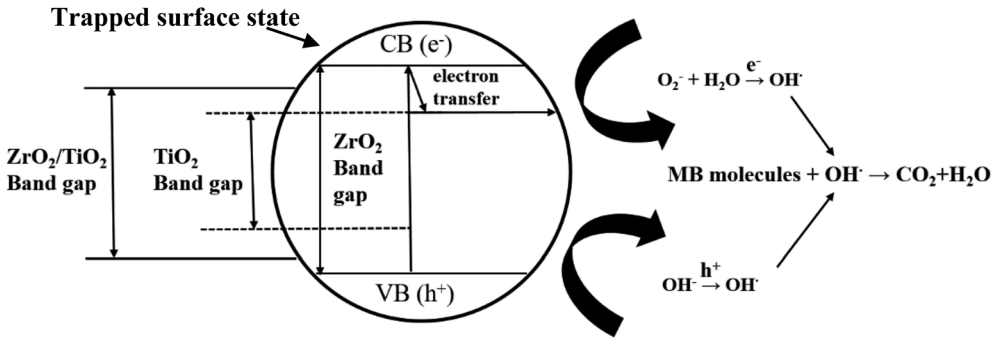

Fig. 8 Proposed mechanism for the photoexcited electron–hole separation and transport processes at the ZrO_2/TiO_2 interface under UV irradiation.

be considered an electrochemical cell, the increase in band gap results in an enhanced oxidation–reduction potential.[19] However, the photocatalytic activity of 60c-Zr/TiO_2 and 80c-Zr/TiO_2 was lower than that of 45c-Zr/TiO_2, despite the band gaps of 60c-Zr/TiO_2 and 80c-Zr/TiO_2 being larger than that of the 45c-Zr/TiO_2 sample. This can be explained by samples with too large a band gap being unable to take full advantage of UV light and therefore being unable to generate enough e^- and h^+ pairs for MB degradation.

Thirdly, there is a fast transfer of the photo-formed electrons from the conduction band (CB) of ZrO_2 to that of TiO_2, when ZrO_2 was deposited on TiO_2 under UV irradiation, since the bottom of the CB edge of ZrO_2 is about 1.3 eV, which is higher than that of TiO_2.[4d,16] This electron transfer prevented radiative electron/hole recombination and thereby improved the photocatalytic activity of the 45c-Zr/TiO_2 sample. In order to evaluate the separation rate of the e^-/h^+ pairs, photoluminescence (PL) analysis was carried out. As shown in Fig. 7, there is only one peak at 433 nm, corresponding to the reflection from the anatase phase of TiO_2. No other peak was observed in the wavelength range of 300–600 nm. With an increase in the number of ZrO_2 ALD cycles, the PL intensity decreased greatly, which indicated that the separation efficiency of the e^-/h^+ pairs was enhanced for the ZrO_2/TiO_2 samples. In other words, the existence of ZrO_2 helped trap the photo-generated charge carriers and inhibited the recombination of the e^-/h^+ pairs. As shown in Fig. 8, e^- and h^+ separation may occur between TiO_2 and ZrO_2 in ZrO_2/TiO_2 since the energy level of TiO_2, for both the valence band (VB) and CB, falls within the band gap of ZrO_2. When the electrons were generated from TiO_2 and ZrO_2, most of the electrons from the CB of ZrO_2 automatically drifted to the CB of TiO_2. Therefore, the e^-/h^+ pair recombination could be inhibited and the photocatalytic activity improved. All factors mentioned above worked collectively and resulted in improved photocatalytic activity of 45c-Zr/TiO_2.

It was also noted that the TiO_2 catalyst containing 1.1 wt% ZrO_2 (45c-Zr/TiO_2) enhanced the photocatalytic activity the most and it was the optimal amount of deposition for the degradation of MB in this study. However, the optimal ZrO_2 amount is not consistent with that reported in the literature, which reported that the optimal ZrO_2 loading was more than 5%. This could be due to the different preparation methods for the ZrO_2/TiO_2 samples.[4a–c] Higher optimal ZrO_2 loading was needed *via* traditional ZrO_2 doping methods because some ZrO_2 was inserted into the interior matrix of the TiO_2 particles and could not work with TiO_2 synergistically. In contrast, in this study, ZrO_2 was highly dispersed on the surface of TiO_2 NPs *via* ALD and thereby the optimal ZrO_2 content was significantly lower. On the other hand, the enlarged band gap of the ZrO_2/TiO_2 samples in this work becomes a limitation and hinders their practical applications under visible light, although ZrO_2 deposition improved the photocatalytic performance of anatase TiO_2 under UV light. N,[20] S,[21] CeO_2[22] and Au/Pd[23] doped TiO_2 catalysts have been reported, and they could decompose organic pollutants under visible light. It is vital and valuable to expand the practical use of TiO_2-based photocatalysts. The optimization and enhancement of ZrO_2/TiO_2 photoactivity under visible light are being pursued by this group.

4. Conclusions

In summary, different numbers of cycles of ALD were used to deposit ZrO_2 on TiO_2 powders. The 45c-Zr/TiO_2 catalyst showed the highest photocatalytic activity and had a more than ten-fold photocatalytic activity enhancement over pure TiO_2 for the degradation of MB under UV light due to the fact that the fast electron transfer from the CB of ZrO_2 to that of TiO_2 prevented radiative electron/hole recombination. This factor worked collectively with another two factors, the maintained high surface area and the larger band gap of ZrO_2/TiO_2, and thus resulted in the significantly improved photocatalytic activity of the samples under UV light. ZrO_2 ALD is a novel and effective strategy to significantly improve the photocatalytic activity of TiO_2, and it is a potentially promising way to enhance the activity of other photocatalysts.

Conflicts of interest

The authors declare no competing financial interest.

Acknowledgements

Acknowledgment is made to the donors of the American Chemical Society Petroleum Research Fund for partial support

of this research. The authors thank Dr Jingjing Qing at the Materials Research Center at Missouri University of Science and Technology for TEM analysis. The authors also thank Naveen K. Mahenderkar and Prof. Jay A. Switzer in the Department of Chemistry for their assistance with diffuse reflectance UV-vis measurement, and Prof. Richard Brow in the Department of Materials Science and Engineering for the assistance with Raman and photoluminescence analysis.

Notes and references

1 (*a*) M. R. Hoffmann, S. T. Martin, W. Choi and D. W. Bahnemann, *Chem. Rev.*, 1995, **95**, 69; (*b*) A. L. Linsebigler, G. Lu and J. T. Yates Jr, *Chem. Rev.*, 1995, **95**, 735; (*c*) Y. Wang, H. Cheng, Y. Hao, J. Ma, W. Li and S. Cai, *J. Mater. Sci.*, 1999, **34**, 3721; (*d*) M. Cao, P. Wang, Y. Ao, C. Wang, J. Hou and J. Qian, *Chem. Eng. J.*, 2015, **264**, 113; (*e*) R. Liu, P. Wang, X. Wang, H. Yu and J. Yu, *J. Phys. Chem. C*, 2012, **116**, 17721.

2 (*a*) X. Wang, T. Li, R. Yu, H. Yu and J. Yu, *J. Mater. Chem. A*, 2016, **4**, 8682; (*b*) M. Cao, P. Wang, Y. Ao, C. Wang, J. Hou and J. Qian, *J. Colloid Interface Sci.*, 2016, **467**, 129.

3 H. Liu, Y. Su, H. Hu, W. Cao and Z. Chen, *Adv. Powder Technol.*, 2013, **24**, 683.

4 (*a*) Y. Gnatyuk, N. Smirnova, A. Eremenko and V. Ilyin, *Adsorpt. Sci. Technol.*, 2005, **23**, 497; (*b*) M. Li, X. Li, G. Jiang and G. He, *Ceram. Int.*, 2015, **41**, 5749; (*c*) B. Neppolian, Q. Wang, H. Yamashita and H. Choi, *Appl. Catal., A*, 2007, **333**, 264; (*d*) X. Qu, D. Xie, L. Cao and F. Du, *Ceram. Int.*, 2014, **40**, 12647; (*e*) C. Sun, L. Liu, L. Qi, H. Li, H. Zhang, C. Li, F. Gao and L. Dong, *J. Colloid Interface Sci.*, 2011, **364**, 288.

5 R. L. Puurunen, *J. Appl. Phys.*, 2005, **97**, 121301.

6 X. Liang and R. L. Patel, *Ceram. Int.*, 2014, **40**, 3097.

7 X. Wang, Y. Jin and X. Liang, *Nanotechnology*, 2017, **28**, 505709.

8 X. Wang, M. Bayan, M. Yu, D. Ludlow and X. Liang, *Int. J. Environ. Sci. Technol.*, 2017, **14**, 1825.

9 K. Naeem and F. Ouyang, *Phys. B*, 2010, **405**, 221.

10 Y. Zhou, D. M. King, X. Liang, J. Li and A. W. Weimer, *Appl. Catal., B*, 2010, **101**, 54.

11 J. Cao, C. Rambo and H. Sieber, *Ceram. Int.*, 2004, **30**, 1967.

12 H. B. Wu, H. H. Hng and X. W. D. Lou, *Adv. Mater.*, 2012, **24**, 2567.

13 S. M. George, *Chem. Rev.*, 2010, **110**, 111.

14 X. Wang, A. R. Donovan, R. L. Patel, H. Shi and X. Liang, *J. Environ. Chem. Eng.*, 2016, **4**, 3767.

15 T. Cao, Y. Li, C. Wang, L. Wei, C. Shao and Y. Liu, *Mater. Res. Bull.*, 2010, **45**, 1406.

16 G. Ramakrishna, A. K. Singh, D. K. Palit and H. N. Ghosh, *J. Phys. Chem. B*, 2004, **108**, 4775.

17 A. Kambur, G. S. Pozan and I. Boz, *Appl. Catal., B*, 2012, **115**, 149.

18 B. M. Pirzada, N. A. Mir, N. Qutub, O. Mehraj, S. Sabir and M. Muneer, *Mater. Sci. Eng., B*, 2015, **193**, 137.

19 C. Zuo, S. Dorris, U. Balachandran and M. Liu, *Chem. Mater.*, 2006, **18**, 4647.

20 (*a*) R. Asahi, T. Morikawa, H. Irie and T. Ohwaki, *Chem. Rev.*, 2014, **114**, 9824; (*b*) G. Wang, X. Xiao, W. Li, Z. Lin, Z. Zhao, C. Chen, C. Wang, Y. Li, X. Huang and L. Miao, *Nano Lett.*, 2015, **15**, 4692; (*c*) Z. Li, F. Wang, A. Kvit and X. Wang, *J. Phys. Chem. C*, 2015, **119**, 4397; (*d*) A. Eslami, M. M. Amini, A. R. Yazdanbakhsh, A. Mohseni-Bandpei, A. A. Safari and A. Asadi, *J. Chem. Technol. Biotechnol.*, 2016, **91**, 2693.

21 (*a*) X. Yan, K. Yuan, N. Lu, H. Xu, S. Zhang, N. Takeuchi, H. Kobayashi and R. Li, *Appl. Catal., B*, 2017, **218**, 20; (*b*) T. Boningari, S. N. R. Inturi, M. Suidan and P. G. Smirniotis, *Chem. Eng. J.*, 2018, **339**, 249; (*c*) S. M. El-Sheikh, G. Zhang, H. M. El-Hosainy, A. A. Ismail, K. E. O'Shea, P. Falaras, A. G. Kontos and D. D. Dionysiou, *J. Hazard. Mater.*, 2014, **280**, 723.

22 D. Tomova, V. Iliev, A. Eliyas and S. Rakovsky, *Sep. Purif. Technol.*, 2015, **156**, 715.

23 A. Cybula, G. Nowaczyk, M. Jarek and A. Zaleska, *J. Nanomater.*, 2014, **2014**, 2.